AQUA
Water Infrastructure, Ecosystems and Society

IWA PUBLISHING

 AQUA — Water Infrastructure, Ecosystems and Society Vol 70 No 6, 856 doi: 10.2166/aqua.2021.034

Using BCN nanostructure as anode electrode for photoelectrocatalytic degradation of organics: a statistical approach

Sadegh Ebadi [a], Karim Ghasemipanah [a], Ebrahim Alaie [a,*], Alimorad Rashidi [b] and Alireza Khataee [c,d]

[a] Environment and Biotechnology Research Division, Research Institute of Petroleum Industry (RIPI), Tehran 14665-137, Iran
[b] Nanotechnology Research Center, Research Institute of Petroleum Industry (RIPI), Tehran 14665-137, Iran
[c] Research Laboratory of Advanced Water and Wastewater Treatment Processes, Department of Applied Chemistry, Faculty of Chemistry, University of Tabriz, Tabriz 51666-16471, Iran
[d] Department of Environmental Engineering, Gebze Technical University, 41400 Gebze, Turkey
*Corresponding author. E-mail: alaiee@ripi.ir

SE, 0000-0002-4437-080X; KG, 0000-0001-6088-0351; EA, 0000-0002-1896-1323; AR, 0000-0001-6753-1939; AK, 0000-0002-4673-0223

ABSTRACT

In this study, boron carbon nitride (BCN) nanostructures were used as a photocatalyst which was synthesized in a chemical vapor deposition reactor. Photoelectrocatalysis was used for degradation organic pollutants from produced water. BCN nanostructures were coated on a coil-type copper wire to act as anode electrode in the photoelectrocatalytic process. The effect of different parameters on chemical oxygen demand (COD) removal efficiency from produced water was investigated by a central composite design (CCD) to maximize photoelectrocatalysis influence as one of the most used methods of wastewater treatment. A 12 run Plackett–Burman design was used for screening of the parameters (initial COD, electrical conductivity, applied cell voltage, UV lamp wavelength, H_2O_2 concentration, residence time, and initial pH) which led to the selection of residence time and initial pH as effective parameters. Since the core goal of this study was to maximize the COD removal efficiency, the steepest ascent method was used to propel these two parameters to the optimum region. Finally, CCD showed that applying photoelectrocatalysis could lead to 88.79% of the COD removal efficiency which would be an optimum value at a residence time of 15.85 min and a pH value of 3.3. Ultimately, this result was confirmed by experimentation at those conditions.

Key words: BCN nanostructure, COD degradation, experimental design, photoelectrocatalysis, produced water

HIGHLIGHTS

- Boron carbon nitride nanomaterials were synthesized as photocatalyst.
- A Plackett–Burman design was used for screening of the effective parameters.
- Chemical oxygen demand (COD) of produced water was decreased by photoelectrocatalysis.
- A central composite design was used for the optimization of COD removal efficiency.

INTRODUCTION

There is too much water inside the oil and gas reservoirs which could appear during the extraction and production operations. This wastewater includes injection, condensed and formation water, and a few treatment chemicals which is called produced water (Xu *et al.* 2016). Produced water contains organic compounds, dissolved, and suspended solids (Guerra & Drewes 2008); hence, it is very hazardous to the environment and its treatment has become a challenge when brought to the surface. The largest volume of wastewater that deals with oil, gas, and petroleum industry can be produced water (Fan *et al.* 2018). About 250 million barrels of produced water was reported to be produced each day in the world in 2015 and its equivalent production of oil was 80 million barrels, which showed that its volume was three times more than the oil volume. For all kinds of produced water, different items such as organics and inorganics, high total dissolved solids (TDS) and consequently high electrical conductivity, and some fatty acids and fouling oil are the common concerns independently of the location (Xu *et al.* 2016).

Different kinds of physical, chemical, and biological treatments such as solvent extraction, adsorption, chemical or biological oxidation, filtration, and advanced oxidation processes (AOPs) have been used for pollutants removal from wastewaters (Ahmadun *et al.* 2009). But most of these processes cannot remove all of the pollutants from produced water efficiently

(Ahmadun *et al.* 2009; Fan *et al.* 2018; Himstedt *et al.* 2018). Therefore, for treating these kinds of complicated wastewaters, some advanced technologies should be developed. Nowadays, photoelectrocatalysis, as one of the AOPs, is used mostly for the enhancement of organic pollutants oxidation. The mechanism of photoelectroctalysis is making electron-hole pairs by disposing of a semiconductor for an energy source such as UV light as shown in reaction (1) and then oxidizing of organics directly by the hole or formation of heterogeneous hydroxyl radicals as powerful oxidation agents (reaction (2)) (Fan *et al.* 2018; Himstedt *et al.* 2018; Meng & Zhang 2018):

$$\text{Semiconductor} + h_\upsilon \rightarrow e^-_{CB} + h^+_{VB} \quad (1)$$

$$h^+_{VB} + H_2O \rightarrow OH^\bullet + H^+ \quad (2)$$

Advanced types of reactors with an immobilized photocatalyst have been recently studied for photoelectrocatalysis. Some researchers showed that these kinds of reactors could degrade different groups of harmful components efficiently (Quan *et al.* 2005; Suhadolnik *et al.* 2016).

Different parameters as independent variables can have effects on pollutants removal from wastewaters as dependent variables (Malvestiti *et al.* 2019). The optimization of the dependent variable is the goal of many studies so does ours. For optimization in conventional methods, all of the independent variables should be kept constant except the one that can vary only one at a time (Hassani *et al.* 2015; Badli *et al.* 2017; Baig *et al.* 2020). So many experiments are needed while using these methods which take more time and cost more (Sharif *et al.* 2016). Experimental design for the modeling and optimization of produced water treatments is an important procedure to promote pollutants removal efficiency while decreasing the number of experiments considerably (Chen *et al.* 2019; Sheikholeslami *et al.* 2019; Shahriari & Hosseini 2020).

In this study, the modeling and optimization of organic pollutants removal processes in produced water treatment were described. Photoelectrocatalysis was used as the treatment process for pollutants degradation, and boron carbon nitride (BCN) nanomaterials were applied as photocatalyst because it has a low bandgap energy (0.5 eV) with respect to current semiconductors (3.02 eV for TiO_2) (Tu *et al.* 2017; Ebadi *et al.* 2021). By using a 12 run Plackett–Burman design as the first step, 2 parameters were screened with 7 main parameters. Following the first step, the steepest ascent method was used for shifting to an optimum region, and finally, a central composite design (CCD) was planned to maximize the response described as chemical oxygen demand (COD) removal efficiency.

MATERIALS AND METHODS

Materials

For photocatalyst (BCN) synthesis, Poly(ethylene glycol)-block-poly(propylene glycol)-block-poly(ethylene glycol) (P123), methanol ($CH_3OH > 99.8\%$), melamine powder, and boric acid as reagent were purchased from Sigma Aldrich. Sulfuric acid and nitric acid (for functionalization of photocatalyst), hydrochloride acid (purity = fuming 37%), sodium hydroxide (for adjusting pH of the wastewater), and acetic acid (for cleaning copper coils before immobilizing of photocatalyst on them), were all Merck index. Copper wire with 250 μm diameter was used as anode and cathode electrodes. The wastewater was sampled from Iranian central oilfields.

Using a MIRA3 TESCAN electronic microscope, electron micrographs were scanned. The analysis of COD was done in a HACH reactor (USA) using $K_2Cr_2O_7$ as oxidant and a DR/200 portable data logging spectrophotometer (HACH, Germany) according to the standard methods for the examination of water and wastewater (Song *et al.* 2016). To determine the structure of the crystal phase of BCN, X-ray diffraction (XRD) was measured using an X'Pert Pro MPD Diffractometer (Panalytical, Netherlands) with radiation of Cu target ($K\propto1$, $\lambda = 1.54$ nm) at 25 °C and 30% RH.

Preparation of catalyst

BCN nanosheets and nanorods were prepared by the chemical vapor deposition (CVD) reactor as follows: P123 (3 g) was added into a stirred solution of demineralized (DM) water and methanol (1:2 volume ratio). When this polymer became completely dissolved, boric acid (3.71 g) and melamine (60.5 g) were added to the solution gently. Approximately 2 h later, a white slurry with high viscosity was gradually formed. During the stirring for 24 h, the temperature of the mixture should be maintained at 50 °C. Finally, obtained white wet cake was transported to the CVD reactor. The temperature of the reactor was set to reach 800 °C with the ramp of 5 °C/min and then was maintained at 800 °C for 3 h. During the reaction, nitrogen gas

purging was used to prevent oxidation reactions at high temperatures. Then the reaction product was cooled overnight by continuing nitrogen gas purging to obtain BCN nanostructures.

Immobilization of catalyst on the electrode

For immobilizing of BCN nanostructures on the copper electrode, first, they should be functionalized to be able to dissolve in water. For functionalizing of these nanostructures, a solution of nitric acid and sulfuric acid (200 mL, 1:3 volume ratio) was evaporated in a balloon and nanostructures got in touch with the vapor on a sintered disc above the balloon for 24 h. Then nanostructures (0.14 g) were dissolved in DM water (50 mL) and stirred for 40 min in an ultrasonic cleaning bath (Clifton) to be dissolved thoroughly. Previously cleaned coil-type copper electrode by acetic acid was immersed in this suspension for 1 h. Finally, the coil was kept inside the oven at 120 °C for 4 h to fabricate anode electrode. Figures 1 and 2 show the XRD and scanning electron microscopy (SEM) of BCN, respectively.

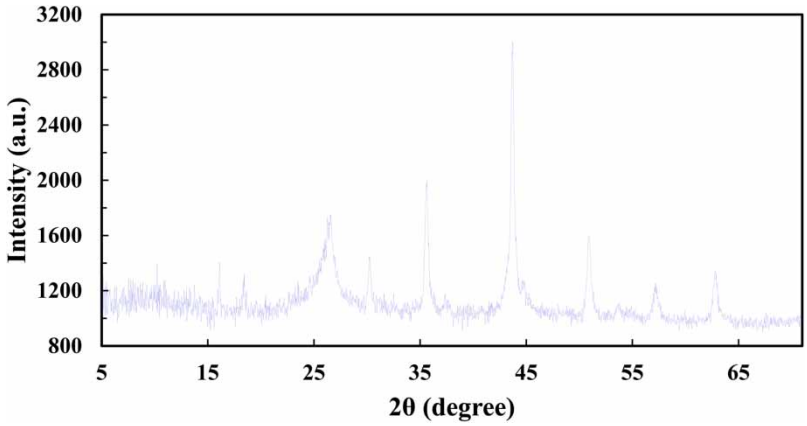

Figure 1 | The XRD pattern of BCN nanosheets and nanorods.

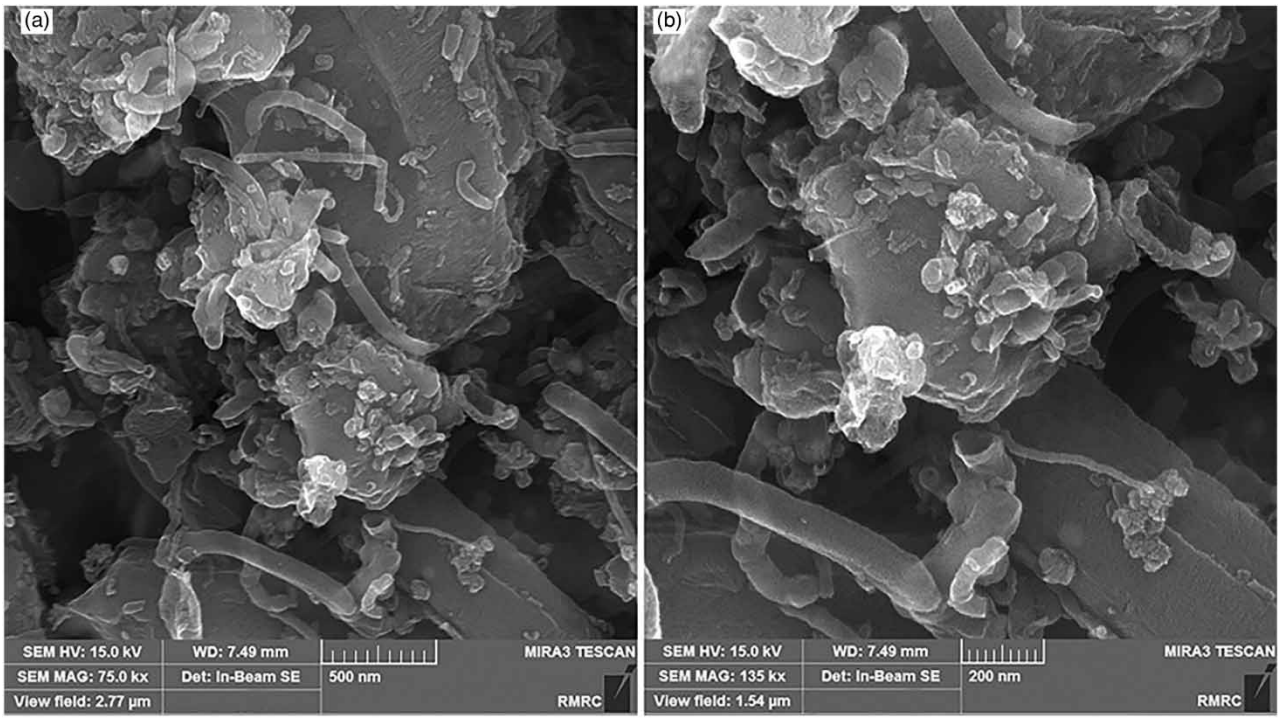

Figure 2 | The SEM images of BCN nanosheets and nanorods: (a) a bar length of 500 nm and (b) a bar length of 200 nm.

Wastewater

The wastewater used in this study was a real case from an Iranian gas field which was distilled first in an evaporation process before using for photoelectrocatalysis. Some characteristics of the wastewater are shown in Table 1.

Experimental apparatus and procedure

The experiments were carried out in an experimental setup. Figure 3 shows the schematic diagram of the experimental setup for COD removal from a gas field produced water by photoelectrocatalysis. The most important section of this setup is the microreactor (3) that includes three coil-type copper electrodes which were placed on a 5 mm outer diameter glass rod inside a UV-transparent 6 mm-inner diameter Plexiglass tube. Two electrodes (12 mm length) were used as cathodes on the sides of the glass rod and one another (64 mm length) which was coated by BCN semiconductor nanostructures was used as an anode on the middle of the glass rod. All of these three electrodes were separated from each other by two 2 mm-length plastic pieces. Wastewater was charged in a 5 mL syringe with a specific diameter and was injected into the microreactor by a syringe pump (SP1000HOM Fnm, Iran) (1). Microreactor was illuminated by two 8 W UV lamps (4 W–365 nm and 4 W–254 nm, VILBER LOURMAT VL-4.LC) (2). An MCH-310D switching DC power supply (China) was used for creating voltage differences between the electrodes (5). The purified wastewater was collected in 10 mL vial bottles (4).

Table 1 | Some properties of gas field produced water

Parameters	Concentration
Conductivity	1,100 μS/cm
TDS	635 mg/L
COD	750 mg/L
BOD	450 mg/L
pH	7.8

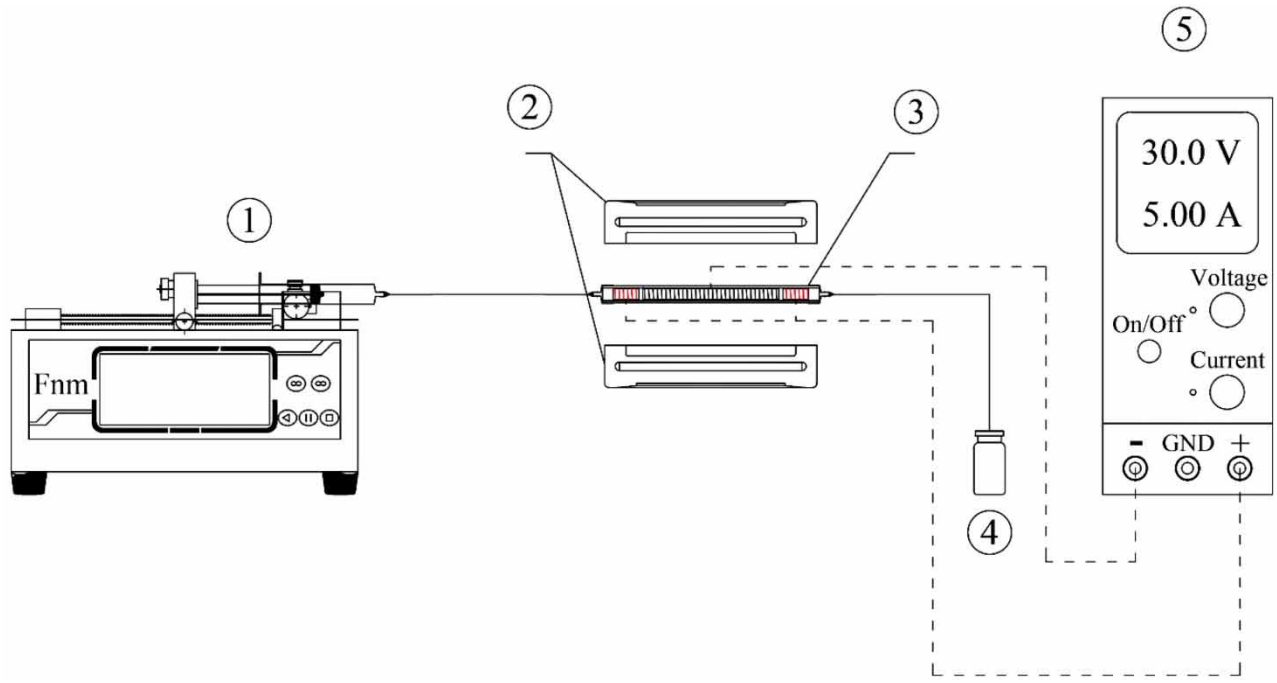

Figure 3 | The experimental setup for organic pollutants removal from gas field produced water by photoelectrocatalysis.

Applied models and experimental design

For each process, different kinds of parameters can have effects on its results. Studying the effect of all parameters separately, which is called one factor at a time, is time-consuming and would be more expensive (Fan *et al.* 2018). However, experimental design can be applied for the identification of significant factors (Kıranşan *et al.* 2015). The Plackett–Burman design is a statistical method that is applied for screening a large number of factors to specify the most effective parameters.

Optimum and valid results with a minimum effort, time, and resources are the primary objectives of applying the experimental design in the analytical process (Kıranşan *et al.* 2015). In an experimental design, response surface methodology (RSM) is a mathematical approach that fits the experimental data to a full-quadratic model, statistically (Nair *et al.* 2014; Myers *et al.* 2016).

RSM was applied to study the effect of residence time (x_1) and pH (x_2) and their interactions on the COD removal efficiency (y). CCD with two variables and three levels was used to obtain the optimum conditions for COD removal. RSM fitted a full-quadratic equation with the experimental data to provide a reasonable response surface modeling through regression analysis. Coded variables (z_i) were used instead of uncoded variables (x_i, $i = 1 - 2$) for studying the effect of different levels of variables (Equation (3)):

$$z_i = \frac{x_i - x_{i.c}}{\Delta x_i} \tag{3}$$

where x_i, $x_{i.c}$, and Δx_i are the virtual amount, virtual amount at the center, and step difference in the variable i ($i = 1 - 2$), respectively. Independent variables in coded levels for RSM design are shown in Table 2.

A second order equation is provided by RSM which includes linear and quadratic variables (Equation (4)):

$$y = \beta_0 + \sum_{i=1}^{2} \beta_i z_i + \sum_{i=1}^{2} \beta_{ii} z_i^2 + \sum_{i=1}^{2} \sum_{j=i+1}^{2} \beta_{ij} z_i z_j + \varepsilon \tag{4}$$

where y represents the response variable (COD removal efficiency), β_0, β_i, β_{ii}, and β_{ij} are regression coefficients for the constant term, the linear term, the square term, and the interaction term, respectively, z_i is a coded variable, and ε is a residual factor associated with the experiments (Bashipour *et al.* 2017).

RESULTS AND DISCUSSION

Photocatalyst

The XRD pattern of photocatalyst in this study (Figure 1) shows that there are nine main reflections in this chart. Reflections that are observed in $2\theta = 26.5$, 43.5, and 50.5 belong to BCN (Tu *et al.* 2017). Three other peaks that occurred in $2\theta = 18.5$,

Table 2 | Independent variables applied in RSM (coded levels)

Run	x_1	x_2
1	1.00	− 1.00
2	− 1.00	− 1.00
3	1.00	1.00
4	− 1.00	1.00
5	1.414	0.00
6	− 1.414	0.00
7	0.00	1.414
8	0.00	− 1.414
9	0.00	0.00
10	0.00	0.00
11	0.00	0.00

30.5, and 35.5 are related to hexagonal boron nitride (h-BN), and other peaks that are seen in $2\theta = 16.5$, 57.5, and 63 show that there is some boron and graphite oxide in the sample (He *et al.* 2013).

The SEM of the nanomaterial shows that most of the particles are in nanosheet and nanorod forms. Nanosheets and nanorods were tied together and made high surfaces, so high energy was adsorbed from UV light by the photocatalyst. Therefore, good results of photoelectrocatalysis efficiency were reached by this combination (Zhou *et al.* 2000; Tu *et al.* 2017).

Analysis of Plackett–Burman design

In this study, the experimental output (y) was COD removal efficiency (%), and parameters for studying their effects on y were initial COD (mg/L), electrical conductivity (μS/cm), applied cell voltage between anode and cathode (V), illuminating UV lamp wavelength (nm), H_2O_2 concentration (mM), hydraulic residence time (min), and initial pH of wastewater (Vinodgopal *et al.* 1996; Cornish *et al.* 2000; An *et al.* 2002; Mao *et al.* 2019). Determining low and high values of each parameter depends on the knowledge about the process. These boundary levels were selected to study if the parameters were effective on y or not. On the other hand, after the Plackett–Burman design, the data should be taken to the optimum region, so boundary levels in this step should be selected around the center of overall boundary levels.

The initial COD of wastewater was 750 mg/L (this is the wastewater that was obtained from the distillation of the main wastewater) and it could be decreased by dilution of the wastewater by DM water. It reached 562.5, 375, and 187.5 mg/L by adding the following amounts of DM water: 25, 50, and 75% of wastewater initial volume, respectively. Finally, 375 and 562.5 mg/L were selected as low and high values of COD. The initial electrical conductivity of wastewater was 1,100 μS/cm and increased to 1,800, 2,500, and 3,300 μS/cm by adding 350, 700, and 1,050 mg/L of NaCl to the wastewater. An average interval should be selected, so 1,800 and 2,500 μS/cm are used as boundary levels. The DC power supply used in this study could create 0–30 V potential differences between electrodes continuously, so 10 and 20 V were used as low and high levels, respectively. Because of the specification of the UV lamp, just two wavelengths (254 and 365 nm) were selected as boundary values of this parameter. According to recent studies, the optimum concentration of H_2O_2 in photoelectrocatalysis is 4–10 mM (An *et al.* 2002; Mao *et al.* 2019). Therefore, it was obvious that 6–8 mM was the best choice of average interval for H_2O_2 concentration. Photoelectrocatalysis is a fast process for the degradation of organic pollutants (Wei & Wan 1991), so the overall time interval was considered to be 5–20 min and between these, 10 and 15 min were considered as boundary levels for the Plackett–Burman design. For safety issues, minimum and maximum values of pH were considered to be 3 and 11, respectively. In this region, the pH values of 5–9 was selected as the central interval for the experimental design.

A 12-experimental PB design was used here, so there were 4 dummy factors labeled as A, C, F, and I which were included randomly in Table 3. The last column in Table 3 represents experimental responses at specified levels of parameters placed in their rows.

By using Equations (1) and (2), the analysis of variance (ANOVA) for the data in Table 3 is summarized in Table 4.

Each of the sum of squares (SS) in Table 4 has just one degree of freedom, so their mean square values (i.e., variances) are the same as the SS ones. The SS values for the dummy factors A, C, F, and I are similarly found to be 6.46, 75.18, 12.88, and 54.04, respectively. The mean SS for these estimates of the random measurement errors is thus 37.14: this has four degrees of freedom, as there are four dummy variables. Each of the individual factors can now be compared with this estimated random error using a one-tailed F-test at the $p = 0.1$ significance level. So for factor initial COD, the value of F is $1.4/37.14 = 0.04$. The critical value of $F_{1,4}$ at $p = 0.1$ is 4.54, so it can be concluded that the effect of changing the level of the initial COD factor is not significant (Myers *et al.* 2016). The same approach shows that the initial pH factor has a significant effect and the residence time factor seems to have a little significant effect. Table 4 shows that the effects of residence time and pH are positive and negative, respectively, which are in agreement with the last research studies (Andand *et al.* 2018; Mansouri *et al.* 2018; Xu *et al.* 2018).

Analysis of RSM

A linear regressive model was derived by applying a current model from the data in Table 3 as Equation (5) (Myers *et al.* 2016):

$$y = 67.80 + 4.15x_1 - 6.16x_2 \tag{5}$$

Table 3 | Different parameter levels and responses for each experiment in the Plackett–Burman design

	Factors											
Run	A	Initial COD (mg/L)	C	Electrical conductivity (μS/cm)	Applied cell voltage (V)	F	UV lamp wavelength (nm)	H_2O_2 concentration (mM)	I	Residence time (min)	Initial pH	*y* (COD removal efficiency) (%)
1	−1	562.5	−1	1,800	10	1	365	8	−1	15	9	55.85
2	1	375	−1	1,800	20	1	365	6	1	15	5	71.20
3	1	375	1	1,800	10	−1	365	8	1	10	9	59.73
4	1	562.5	1	1,800	20	1	254	8	−1	10	5	67.29
5	−1	375	−1	2,500	20	1	254	8	1	10	9	54.80
6	1	562.5	−1	2,500	20	−1	365	6	−1	10	9	48.27
7	1	375	1	2,500	10	1	254	6	−1	15	9	64.53
8	−1	562.5	1	1,800	20	−1	254	6	1	15	9	74.99
9	−1	562.5	1	2,500	10	1	365	6	1	10	5	73.10
10	1	562.5	−1	2,500	10	−1	254	8	1	15	5	78.19
11	−1	375	1	2,500	20	−1	365	8	−1	15	5	75.29
12	−1	375	−1	1,800	10	−1	254	6	−1	10	5	67.02

Table 4 | ANOVA for the Plackett–Burman design

Factor	Effect	SS	*F*-value
A	− 1.94	6.46	…
Initial COD (mg/L)	0.90	1.40	0.04
C	6.62	75.18	…
Electrical conductivity (μS/cm)	− 0.34	0.20	0.01
Applied cell voltage (V)	− 1.14	2.23	0.06
F	− 2.74	12.88	…
UV lamp wavelength (nm)	− 3.84	25.24	0.68
H_2O_2 concentration (mM)	− 1.35	3.12	0.08
I	5.61	54.04	…
Residence time (min)	8.31	118.41	3.19
Initial pH	− 12.31	259.82	7.00

where y is the response and x_1 and x_2 are the coded variables which represent residence time and initial pH, respectively. Considering low and high levels of these parameters as mentioned above, it is concluded that:

$$x_1 = \frac{\xi_1 - 12.5}{2.5} \tag{6}$$

$$x_2 = \frac{\xi_2 - 7}{2} \tag{7}$$

where ξ_1 and ξ_2 are the pH and residence time, respectively. If Δx_1 was considered to be 0.5, by using Equations (5)–(7) Δx_2, $\Delta\xi_1$, and $\Delta\xi_2$ would be as follows:

$$\Delta x_2 = \frac{-6.16}{4.15}\Delta x_1 = -0.74 \tag{8}$$

$$\Delta\xi_1 = 2.5\Delta x_1 = 1.25 \tag{9}$$

$$\Delta\xi_2 = 2\Delta x_2 = -1.48 \tag{10}$$

Table 5 shows the different steps of the steepest ascent.

Considering that pH could not be decreased to less than 3, doing the experiment correspondent to origin + 3Δ was impossible. The last row of Table 5 belongs to a pH value of 3 which was obtained by interpolation between origin + 2Δ and origin + 3Δ. It is obvious from Table 5 that y is continuously increased with increasing residence time and decreasing pH. Finally, when residence time is 15.88 min and pH is 3.00, y starts to decrease so a step before that (residence time: 15.00 min and pH: 4.04) is the optimum region and a CCD should be designed around this point for the response optimization.

Optimizing of operating conditions

A CCD was used in the optimum region that was obtained by the steepest ascent in the above section for optimizing the response as shown in Table 6. A second-order regressive model including interactions and curvature was derived by applying a current model from the data in Table 6 as Equation (11) (Myers *et al.* 2016):

$$y = 84.46 + 3.07x_1 - 2.58x_2 - 1.96x_1^2 - 0.46x_2^2 - 0.99x_1x_2 \tag{11}$$

where x_1 and x_2 are representative for residence time and pH, respectively, and are defined as Equations (12) and (13):

$$x_1 = \frac{\xi_1 - 15}{0.75} \tag{12}$$

$$x_2 = \frac{\xi_2 - 4.04}{0.5} \tag{13}$$

Table 5 | Different parameter levels and responses for each experiment in the steepest ascent method

					y (COD removal efficiency) (%)	
Step	x_1	x_2	ξ_1	ξ_2	**Predicted**	**Experimental**
Origin	0.00	0.00	12.50	7.00	67.80	65.85
Origin + Δ	0.50	− 0.74	1.25	− 1.48	…	…
Origin + 2Δ	0.50	− 0.74	13.75	5.52	74.43	79.36
Origin + 3Δ	1.00	− 1.48	15.00	4.04	81.07	84.65
Origin + 3Δ	1.50	− 2.22	16.25	2.56	87.70	…
…	1.35	− 2.00	15.88	3.00	85.72	82.53

Table 6 | Different parameters levels and responses for each experiment in CCD

					y (COD removal efficiency) (%)	
Run	x_1	x_2	ξ_1	ξ_2	**Experimental**	**Predicted**
1	1.00	− 1.00	15.75	3.54	87.32	88.60
2	− 1.00	− 1.00	14.25	3.54	80.24	80.48
3	1.00	1.00	15.75	4.54	82.34	81.62
4	− 1.00	1.00	14.25	4.54	79.21	77.46
5	1.14	0.00	16.06	4.04	85.38	84.88
6	− 1.14	0.00	13.94	4.04	75.23	76.20
7	0.00	1.14	15.00	4.75	78.14	80.00
8	0.00	− 1.14	15.00	3.33	88.50	87.08
9	0.00	0.00	15.00	4.04	84.65	84.46
10	0.00	0.00	15.00	4.04	82.70	84.46
11	0.00	0.00	15.00	4.04	86.04	84.60

The predicted responses by the regressive model (Equation (11)) are shown in the last column of Table 6 that indicates good adaptability with experimental *y*.

ANOVA for this design (CCD) is summarized in Table 7.

Analytical optimization by RSM predicts optimum *y*. Some independent variables, which resulted in maximum *y* (89.76%), were estimated by RSM. These variables were applied to fix the optimum conditions for maximum *y*. The greatest amount of *y* was predicted at a residence time of 15.86 min and an initial pH value of 3.33. An experiment was done in these conditions and resulted in 89.00% of COD removal efficiency which was in good agreement with the predicted value.

Contour and surface plots of COD removal efficiency versus residence time and pH are shown in Figures 4 and 5, respectively.

CONCLUSION

In this study, the design and manufacture of a microreactor with BCN as photocatalyst was explained thoroughly. This paper is aimed to use experimental design for the optimization of organics removal from a gas field produced water by photoelectrocatalysis. A 12 run Plackett–Burman experimental design was used for determining the most influential parameters by screening 7 different factors and results, which indicated that the following two parameters had significant effects on this process: residence time and initial pH. A linear predictive model was derived from the experimental results of Plackett–Burman

Table 7 | ANOVA for CCD

Source	Degree of freedom	Sequential sum of squares	Adjusted sum of squares	Adjusted mean squares	*F*	*P*
Regression	5	154.537	154.537	30.907	8.81	0.02
Linear	2	128.786	128.786	64.393	18.35	0.01
Square	2	21.850	21.850	10.925	3.11	0.13
Interaction	1	3.901	3.901	3.901	1.11	0.34
Residual effect	5	17.543	17.543	3.509		
Lack of fit	3	11.913	11.913	3.971	1.41	0.44
Pure error	2	5.630	5.630	2.815		
Total	10	172.080				

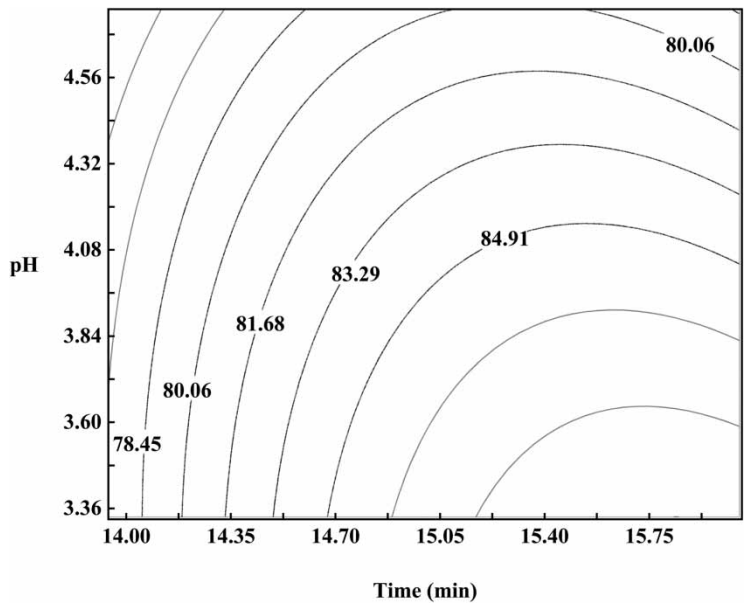

Figure 4 | Contour plot of residence time and pH at constant COD removal efficiencies.

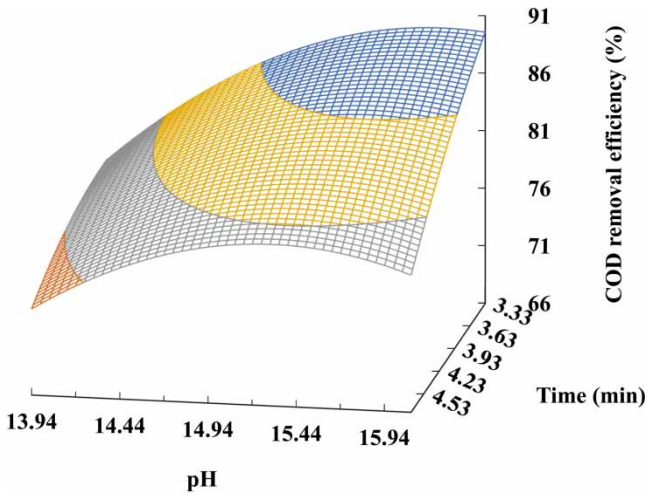

Figure 5 | Surface plot of COD removal efficiency versus residence time and pH.

design which its predicted values were in good agreement with experimental results. As COD removal efficiency was the target parameter for reviewing the influence of the photoelectrocatalysis process on organic pollutants removal, so the steepest ascent was used to maximize this parameter. The steepest ascent was used as a technique for taking selected parameters to the optimum region.

A CCD with 11 runs was applied to optimize the significant parameters obtained by the Plackett–Burman design. A polynomial regression model was obtained from CCD experimental responses which included individual parameters and their interactions. This model predicted values that were also in good agreement with experimental responses. The predicted results showed that the maximum COD removal of 88.79% could be achieved with a residence time of 15.68 min and a pH value of 3.54. The predicted values were in agreement with experimental values with a coefficient of determination (R^2) of 0.90. The model was validated by subsequent experimentations at the optimized conditions.

ACKNOWLEDGEMENTS

We thank Mr Akbar Irandokht for his assistance in preparing this article. The authors are also grateful for the support provided by the Research Institute of Petroleum Industry (RIPI) in Iran.

DATA AVAILABILITY STATEMENT

All relevant data are included in the paper or its Supplementary Information.

REFERENCES

Ahmadun, F. R., Pendashteh, A., Abdullah, L. C., Biak, D. R. A., Madaeni, S. S. & Zainal Abidin, Z. 2009 Review of technologies for oil and gas produced water treatment. *Journal of Hazardous Materials* **170**, 530–551. https://doi.org/10.1016/j.jhazmat.2009.05.044.

An, T. C., Zhu, X. H. & Xiong, Y. 2002 Feasibility study of photoelectrochemical degradation of methylene blue with three-dimensional electrode-photocatalytic reactor. *Chemosphere* **46**, 897–903. https://doi.org/10.1016/S0045-6535(01)00157-6.

Andand, A., Singh, G. & Saraf, S. A. 2018 Plackett–Burman design as a tool for screening and process optimization of rivastigmine-loaded lipid nanoparticles. *Asian Journal of Pharmaceutical and Clinical Research* **11** (12), 155–158. http://dx.doi.org/10.22159/ajpcr.2018.v11i12.28066.

Badli, N. A., Ali, R., Abu Bakar, W. A. W. & Yuliati, L. 2017 Role of heterojunction $ZrTiO_4/ZrTi_2O_6/TiO_2$ photocatalyst towards the degradation of paraquat dichloride and optimization study by Box–Behnken design. *Arabian Journal of Chemistry* **10**, 935–943. https://doi.org/10.1016/j.arabjc.2016.02.011.

Baig, U., Uddin, M. K. & Gondal, M. A. 2020 Removal of hazardous azo dye from water using synthetic nano adsorbent: facile synthesis, characterization, adsorption, regeneration and design of experiments. *Colloids and Surfaces A: Physicochemical and Engineering Aspects* **584**, 124031. https://doi.org/10.1016/j.colsurfa.2019.124031.

Bashipour, F., Rahimi, A., Nouri Khorasani, S. & Naderinik, A. 2017 Experimental optimization and modeling of sodium sulfide production from H_2S-rich off-gas via response surface methodology and artificial neural network. *Oil & Gas Science and Technology* **72**. https://doi.org/10.2516/ogst/2017004.

Chen, X., Huang, G., An, C., Feng, R., Yao, Y., Zhao, S., Huang, C. & Wu, Y. 2019 Plasma-induced poly(acrylic acid)-TiO_2 coated polyvinylidene fluoride membrane for produced water treatment: synchrotron X-ray, optimization, and insight studies. *Journal of Cleaner Production* **227**, 772–783. https://doi.org/10.1016/j.jclepro.2019.04.226.

Cornish, B. J. P. A., Lawton, L. A. & Robertson, P. K. J. 2000 Hydrogen peroxide enhanced photocatalytic oxidation of microcystin-LR using titanium dioxide. *Applied Catalysis B: Environmental* **25**, 59–67. https://doi.org/10.1016/S0926-3373(99)00121-6.

Ebadi, S., Ghasemipanah, K., Alaie, E., Rashidi, A. & Khataee, A. 2021 COD removal from gas field produced water using photoelectrocatalysis process on coil type microreactor. *Journal of Industrial Engineering and Chemistry* **98**, 262–269. https://doi.org/10.1016/j.jiec.2021.03.045.

Fan, M., Hua, J., Cao, R., Ruan, W. & Wei, X. 2018 A review on experimental design for pollutants removal in water treatment with the aid of artificial intelligence. *Chemosphere* **200**, 330–343. https://doi.org/10.1016/j.chemosphere.2018.02.111.

Guerra, K. & Drewes, J. E. 2008 Produced water in the western United States: geographical distribution, occurrence, and composition. *Environmental Engineering Science* **25**, 239–246. https://doi.org/10.1089/ees.2007.0026.

Hassani, A., Khataee, A., Karaca, S., Karaca, M. & Kıranşan, M. 2015 Adsorption of two cationic textile dyes from water with modified nanoclay: a comparative study by using central composite design. *Journal of Environmental Chemical Engineering* **3** (4), 2738–2749. https://doi.org/10.1016/j.jece.2015.09.014.

He, X., Joo, S., Xiao, H. & Liang, H. 2013 Boron-based nanoparticles for chemical-mechanical polishing of copper films. *ECS Journal of Solid State Science and Technology* **2**, 20–25. https://doi.org/10.1149/2.021301jss.

Himstedt, H. H., Sengupta, A., Qian, X. & Wickramasinghe, S. R. 2018 Magnetically responsive nano filtration membranes for treatment of coal bed methane produced water. *Journal of the Taiwan Institute of Chemical Engineering* **94**, 97–108. https://doi.org/10.1016/j.jtice.2018.01.007.

Kıranşan, M., Khataee, A., Karaca, S. & Sheydaei, M. 2015 Artificial neural network modeling of photocatalytic removal of a disperse dye using synthesized of ZnO nanoparticles on montmorillonite. *Spectrochimica Acta Part A: Molecular and Biomolecular Spectroscopy* **140**, 465–473. https://doi.org/10.1016/j.saa.2014.12.100.

Malvestiti, J. A., Fagnani, E., Simao, D. & Dantas, R. F. 2019 Optimization of UV/H2O2 and ozone wastewater treatment by the experimental design methodology. *Environmental Technology* **40** (15), 1910–1922. https://doi.org/10.1080/09593330.2018.1432698.

Mansouri, M., Elhammoudi, N., Aboul-hrouz, S., Mouiya, M., Makouki, L., Chham, A., Abourriche, A., Hannache, H. & Oumam, M. 2018 Elaboration of novel adsorbent from Moroccan oil shale using Plackett–Burman design. *Chemistry International* **4** (1), 7–14.

Mao, Y., Li, Y., Zou, Y., Shen, X., Zhu, L. & Lia, G. 2019 Solvothermal synthesis and photocatalytic properties of ZnO micro/nanostructures. *Ceramics International* **45** (2), 1724–1729. https://doi.org/10.1016/j.ceramint.2018.10.054.

Meng, X. & Zhang, Z. 2018 Two dimensional graphitic materials for photoelectrocatalysis: a short review. *Catalysis Today* **315**, 2–8. https://doi.org/10.1016/j.cattod.2018.03.015.

Myers, R. H., Montgomery, D. C. & Anderson-Cook, C. M. 2016 *Response Surface Methodology: Process and Product Optimization Using Designed Experiments*, 4th edn. John Wiley & Sons, Hoboken, NJ.

Nair, A. T., Makwana, A. R. & Ahammed, M. M. 2014 The use of response surface methodology for modeling and analysis of water and wastewater treatment processes: a review. *Water Science & Technology* **69** (3), 464–478. https://doi.org/10.2166/wst.2013.733.

Quan, X., Yang, S., Ruan, X. & Zhao, H. 2005 Preparation of titania nanotubes and their environmental applications as electrode. *Environmental Science & Technology* **39**, 3770–3775. https://doi.org/10.1021/es048684o.

Shahriari, H. R. & Hosseini, S. S. 2020 Experimental and statistical investigation on fabrication and performance evaluation of structurally tailored PAN nanofiltration membranes for produced water treatment. *Chemical Engineering and Processing – Process Intensification* **147**, 107766. https://doi.org/10.1016/j.cep.2019.107766.

Sharif, K. M., Rahman, M. M., Azmir, J., Mohamed, A., Jahurul, M. H. A., Sahena, F. & Zaidul, I. S. M. 2016 Experimental design of supercritical fluid extraction – a review. *Journal of Food Engineering* **124**, 105–116. http://dx.doi.org/10.1016/j.jfoodeng.2013.10.003.

Sheikholeslami, Z., Yousefi Kebria, D. & Qaderi, F. 2019 Investigation of photocatalytic degradation of BTEX in produced water using γ-Fe_2O_3 nanoparticle. *Journal of Thermal Analysis and Calorimetry* **135**, 1617–1627. https://doi.org/10.1007/s10973-018-7381-x.

Song, G., Xi, H. & Zhou, Y. 2016 Determination of forty pollutants in wastewater by liquid–liquid extraction and gas chromatography–mass spectrometry. *Analytical Letters* **49**, 1480–1491. http://dx.doi.org/10.1080/00032719.2015.1116005.

Suhadolnik, L., Pohar, A., Likozar, B. & Čeh, B. 2016 Mechanism and kinetics of phenol photocatalytic, electrocatalytic and photoelectrocatalytic degradation in a TiO_2-nanotube fixed-bed microreactor. *Chemical Engineering Journal* **303**, 292–301. http://dx.doi.org/10.1016/j.cej.2016.06.027.

Tu, W., Xu, Y., Wang, J., Zhang, B., Zhou, T., Yin, S., Wu, S., Li, C., Huang, Y., Zhou, Y., Zou, Z., Robertson, J., Kraft, M. & Xu, R. 2017 Investigating the role of tunable nitrogen vacancies in graphitic carbon nitride nanosheets for efficient visible-light-driven H_2 evolution and CO_2 reduction. *ACS Sustainable Chemistry Engineering* **5**, 7260–7268. https://doi.org/10.1021/acssuschemeng.7b01477.

Vinodgopal, K., Bedja, I. & Kamat, P. V. 1996 Nanostructured semiconductor films for photocatalysis. photoelectrochemical behavior of SnO_2/TiO_2 composite systems and its role in photocatalytic degradation of a textile azo dye. *Chemistry of Materials* **8**, 2180–2187. https://doi.org/10.1021/cm950425y.

Wei, T. Y. & Wan, C. C. 1991 Hetrogeneous photocatalytic oxidation of phenol with titanium dioxide powders. *Industrial & Engineering Chemistry Research* **30**, 1293–1300. https://doi.org/10.1021/ie00054a033.

Xu, Y., Shen, D., Dong, B. & Dai, X. 2016 A new strategy for reusing the oilfield-produced water as boiler feedwater without desilication. *Journal of the Taiwan Institute of Chemical Engineering* **68**, 169–172. http://dx.doi.org/10.1016/j.jtice.2016.08.031.

Xu, Q. S., Xu, Y. D., Li, L. & Fang, K. T. 2018 Uniform experimental design in chemometrics. *Journal of Chemometrics*. https://doi.org/10.1002/cem.3020.

Zhou, Z. F., Bello, I., Lei, M. K., Li, K. Y., Lee, C. S. & Lee, S. T. 2000 Synthesis and characterization of boron carbon nitride films by radio frequency magnetron sputtering. *Surface and Coatings Technology* **128–129**, 334–340. https://doi.org/10.1016/S0257-8972(00)00600-9.

First received 2 March 2021; accepted in revised form 28 July 2021. Available online 10 August 2021